LANGMUIR

pubs.acs.org/Langmuir Article

Rupture of Liquid Bridges on Porous Tips: Competing Mechanisms of Spontaneous Imbibition and Stretching

Si Suo and Yixiang Gan*

Cite This: *Langmuir* 2020, 36, 13642−13648 Read Online

ACCESS | Metrics & More | Article Recommendations

ABSTRACT: Liquid bridges are commonly encountered in nature and the liquid transfer induced by their rupture is widely used in various industrial applications. In this work, with the focus on the porous tip, we studied the impacts of capillary effects on the liquid transfer induced by the rupture through numerical simulations. To depict the capillary effects of a porous tip, a time scale ratio, R_T, is proposed to compare the competing mechanisms of spontaneous imbibition and external drag. In terms of R_T, we then develop a theoretical model for estimating the liquid retention ratio considering the geometry, porosity, and wettability of tips. The mechanism presented in this work provides a possible approach to control the liquid transfer with better accuracy in microfluidics or microfabrications.

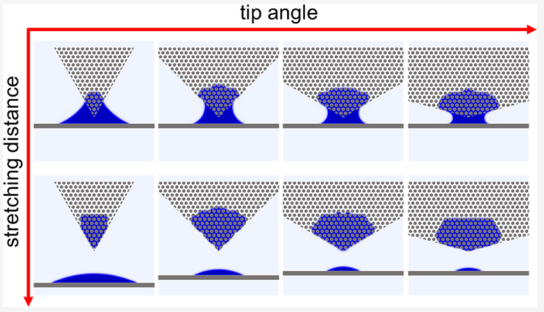

INTRODUCTION

The dynamics of a liquid bridge formed between two surfaces are referred to as a fluid−solid interaction dominated by capillary effects. Specifically, formation and breakup of liquid bridges can be controlled by kinetic conditions, fluid properties, surface wettability, and morphology.[1−5] Although the morphology of adhered surfaces plays an important role in the movement of a three-phase contact line,[6,7] there is increasing interest in achieving sufficient understanding of their effects on the rupture of liquid bridges.[8] Especially for cases with permeable surfaces, the competing mechanisms of spontaneous imbibition and menisci deformation can give rise to interesting phenomena.[9−11]

Liquid bridges are ubiquitous in nature and well studied in various industries. In wetted granular materials, e.g., wet sandy soil and humid powders, the capillary force generated by liquid bridges induces grain−grain cohesion, resulting in the increment of shear strength,[12] grain agglomerations,[13] and self-assembly.[14] With industrial applications, capillary forces generated by the liquid meniscus between a gripper and objects can be used to handle tiny components,[15] e.g., watch bearings.[16] This capillary gripping presents significant advantages over the tiny-scale manipulations, such as indirect contact with the objects, self-centering, and high compatibility with various shapes and materials. However, it is required that the amount of remaining liquid on the object is as small as possible.[8] Conversely, for the atomic force microscopy (AFM) technique, the liquid bridge between the probe and object resulting from a humid ambience should be eliminated as much as possible to enhance the imaging resolution.[17] Under dynamic conditions, liquid bridges can also be formed between the dip and the substrate in a variety of transfer printing processes,[18] e.g., off-set printing,[19] gravure,[20] lithography,[21] and so on. The basic technique for printing is to control the liquid volume transferred from one surface to another. In microfluidics, such as those used in chemical engineering and biological sciences, there is a general need to accurately manipulate a droplet, and liquid bridges are usually adopted as a tool to merge, transport, or reshape droplets.[22−24] In these applications, designing a controllable liquid transfer between two surfaces is a basic requirement for various industrial applications.

To date, there have been numerous studies investigating mechanisms of rupture-induced liquid transfer between two solid substrates. Specifically, this phenomenon can be divided into two regimes according to the stretching speed.[25,26] One is the dynamic regime, where viscous and inertial forces dominate and therefore the liquid bridge can be almost equally separated regardless of other conditions; the other is the quasi-static regime, where capillary force dominates, so the liquid transfer is determined by a combination of surface wettability properties. Theoretical solutions for the maximum stretching distance or the minimum liquid value of a liquid bridge have been developed based on the Young−Laplace equation[27−29] and free energy.[30] Some meniscus-shape-based models for simplicity have also been developed, i.e., assuming a

Received: August 21, 2020
Revised: October 16, 2020
Published: November 4, 2020

https://dx.doi.org/10.1021/acs.langmuir.0c02479
Langmuir 2020, 36, 13642−13648

parabolic[31] or elliptical[32] shape for the gas−liquid interface. However, many existing studies mainly focus on the simple geometrical configurations, i.e., plane to plane,[33] sphere to sphere,[27,34] or sphere to plane.[35,36] A recent study by Tourtit et al.[8] suggests that the surface geometry is another controlling condition for the quasi-static regime, and the relationship between the tip angle of a gripper and its liquid retention has been established.

In many applications, substrates for liquid transfer are often porous. Porous media, e.g., paper, open-cell foams, and fabrics, usually work as desirable multiphase flow controllers since their capillary effects can be tuned by changing porous properties, i.e., porosity, pore size, etc.[37−39] Therefore, the controllability of porous media has led to a series of applications, like paper-based chips and[40,41] gas diffusion layers in fuel cells.[42] Based on our previous work,[43] which concludes that the surface geometry together with the porous structure determines the behavior of a sessile droplet moving on a porous surface, here, we further explore the porous structure as grippers for manipulating the dynamics of liquid bridges. The focus of our work is to investigate how porous properties influence the liquid transfer induced by the liquid bridge rupture within a quasi-static regime. This paper is arranged as follows: the numerical scheme is first introduced and validated against an experimental work; then, by combining the main controlling factors including stretching speed, surface wettability, and porous properties, a scaling parameter, the time ratio R_T, is proposed to compare the two main competing mechanisms of spontaneous imbibition and external stretching, and an estimation of liquid retention ratio L_r in terms of R_T is performed based on the simulation results. Finally, controlling liquid transfer with better accuracy and wider range using this model is discussed.

NUMERICAL METHOD

To exactly capture the capillary effect within a porous zone, we implemented pore-scale-resolved models using the phase field numerical scheme. The porous media are realized by a series of homogeneous arrangements of two-dimensional (2D) circular obstacles to explicitly model the pore structures. The interface movement and splitting inside and outside the porous zone and its adhesion with solid boundaries are captured based on the phase field method.

Phase Field Method for Multiphase Flow. The phase field method combines the Navier−Stokes equation with the Cahn−Hilliard diffusion equation[44−47]

$$\nabla \cdot u = 0 \tag{1}$$

$$\frac{\partial(\rho \mathbf{u})}{\partial t} + \nabla \cdot (\rho \mathbf{u}\mathbf{u}) - \nabla \cdot (\boldsymbol{\mu} \nabla \mathbf{u}) - \nabla \mathbf{u} \cdot \nabla \mu = -\nabla p + \mathbf{F}_{st} + \mathbf{F}_{ext} \tag{2}$$

$$\frac{\partial \vartheta}{\partial t} + \mathbf{u} \cdot \nabla \vartheta = \nabla \cdot \frac{\gamma \lambda}{\varepsilon^2} \nabla \psi \tag{3}$$

$$\psi = -\nabla \cdot \varepsilon^2 \nabla \vartheta + (\vartheta^2 - 1)\vartheta \tag{4}$$

where p is the pressure, $\mathbf{u}$ is the fluid velocity field, μ is the fluid viscosity of fluid, $\mathbf{F}_{ext}$ is the external body force, e.g., the gravity, ϑ is the phase variable, which varies in the range $[-1, 1]$, i.e., $\vartheta = 1$ in the pure gas phase and $\vartheta = -1$ in the pure liquid phase, γ is the mobility parameter, ψ is a modified chemical potential that decomposes a fourth-order equation into two second-order equations, λ is the mixing energy density, and ε is a control parameter for the interface thickness that scales with the thickness of the interface. The parameters λ and ε are related to surface tension σ through the equation

$$\sigma = \frac{2\sqrt{2}\lambda}{3\varepsilon^2} \tag{5}$$

and the surface tension effect can be considered as a body force $\mathbf{F}_{st}$ as

$$\mathbf{F}_{st} = \frac{\lambda \psi}{\varepsilon^2} \nabla \vartheta \tag{6}$$

In the phase field model, the interfacial thickness ε and mobility γ are two particularly important parameters. A smaller interfacial thickness ε requires typically a much finer mesh, thus leading to a great increase in computational cost and causing difficulties in convergence with the phase field method, though it would be close to the solution with a sharp-interface assumption. Therefore, the value of ε should be related to the current mesh size and recommended to be half of the maximum mesh size. For any given value of ε, according to the expression of surface tension σ, the mixing energy density λ can be obtained by eq 5. The mobility parameter γ determines the time scale of the Cahn−Hilliard diffusion, and it thereby governs the diffusion-related time scale for the interface. A suitable value for γ is the maximum velocity magnitude occurring in the model and higher mobility is helpful to obtain the correct pressure variation crossing the interface while the simulations may suffer from numerical convergency issues if γ is chosen to be too large. To balance numerical convergency and accuracy, in the following simulations, we use $\varepsilon = 0.1$ mm and mobility $\gamma = 0.1$ m·s/kg, which can guarantee that the liquid mass inconsistency throughout the simulation is less than 0.5% of the initial droplet mass.

The wettability condition of solid boundaries, in this numerical scheme, can be applied by two steps: (1) truncate phase diffusion along the normal of solid boundaries and (2) modify the local normal to the interface contacting the solid boundaries, and specifically by implementing

$$\mathbf{n} \cdot \nabla \psi = 0 \tag{7}$$

$$\mathbf{n} \cdot \frac{\nabla \vartheta}{|\nabla \vartheta|} = \cos(\theta) \tag{8}$$

where θ is the contact angle measured within the liquid phase. Equations 1−4 and their boundary and initial conditions are implemented in the commercial FEA software, Comsol, and additionally, the motion of solid boundaries can be realized with the help of a moving mesh module.

Validation. The recent experimental work by Tourtit et al[8] systematically presented the rupture of a liquid bridge between a solid tip and a plane, and thus provides a clear possibility to validate the numerical scheme. Here, the rupture process of a liquid bridge is tracked in a 2D computational domain, and related fluid properties and environmental conditions can be found in ref 8. Though an axisymmetric domain seems to be more suitable to model these conical tips, we did not see the difference between the results obtained in the current domain and axisymmetric approximations. The former is adopted since later while modeling porous media, the 2D simplification can straightforwardly reflect the porous structure. Notably, another simplification is that the reference equilibrium contact angle is adopted here without considering the contact angle hysteresis

https://dx.doi.org/10.1021/acs.langmuir.0c02479
Langmuir 2020, 36, 13642−13648

and dynamics,[48] which might be a contributing factor to the difference between the simulation and experimental results. The liquid retention ratio L_r, i.e., a ratio of liquid volume left on the tip and initial droplet volume when the liquid bridge ruptures, with respect to different tip angles is presented in Figure 1 and compared with the experimental data. As shown

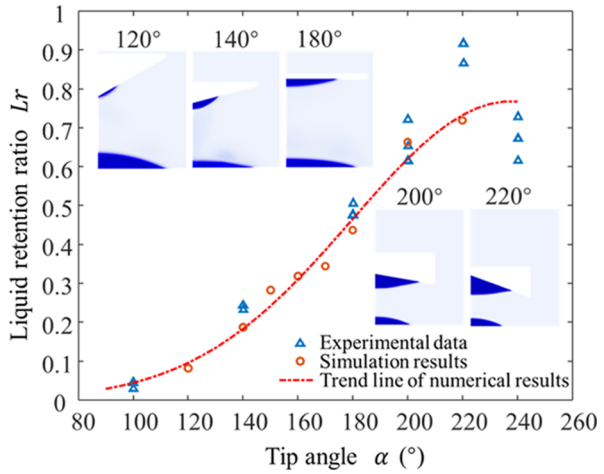

Figure 1. Numerical validation against experimental data for liquid retention ratio L_r with respect to the tip angle α.

in Figure 1, most numerical results are in good agreement with the experimental results, except for the cases with the tip angle larger than 200°, while the experimental data also shows higher variance for these cases. Overall, our simulation results can follow the experimentally observed behaviors demonstrated in ref 8, and furthermore, the phase field method with the moving mesh technique can capture the dynamics of liquid bridges.

Modeling the Porous Structure and Flow Conditions. In this study, we mainly investigate the effect of the porous structure on liquid retention, and therefore fluid properties of the liquid−gas system are fixed in all numerical cases while varying the porous geometry and wettability. A schematic of the present numerical model is shown in Figure 2. Our simulation is on a 2D symmetric domain including a porous zone that is dry initially. The liquid droplet with an initial radius r_d = 5 mm is dropped on a solid plane that is moved along the vertical direction. The solid plane moves upward a certain distance (1 mm) to guarantee that the droplet touches the porous tip and the liquid bridge forms between the solid and porous substrates. Then, the solid plane moves downward at a constant speed until the liquid bridge breaks up. A typical water−air system is assumed, in which liquid viscosity $\mu_l = 1 \times 10^{-2}$ Pa·s and density ρ_l = 1000 kg/m^3, while gas viscosity $\mu_g = 1.85 \times 10^{-5}$ Pa·s and ρ_g = 1.2 kg/m^3; the surface tension σ between these two fluids equals 72.9 mN/m. To guarantee that the capillary effect controls the whole process instead of the viscosity, the moving speed u of the solid plane is kept lower than 4 mm/s so that the capillary number $Ca = \frac{\mu_l u}{\sigma} < 5.6 \times 10^{-5}$.

As for the geometry of porous tips, microscopically, the circular obstacles inside the porous tips are arranged on regular hexagonal grids, which can be considered as the simplest representation of homogeneous porous media. Here, we fix the center-to-center distance l_c =1 mm between two neighboring obstacles and change the obstacle size to adjust the porosity ϕ (0.42 and 0.49) and correspondingly throat size d (0.2 and 0.25 mm) of porous zones; macroscopically, the shape of the porous zone varies from a sharp wedge to a blunt tip and finally to a plate and is controlled by the tip angle α ranging from 60 to 180°. The contact angle of the porous zone θ covers a range from 30 to 45 and 60°, i.e., from strong imbibition to weak imbibition, while the contact angle for the solid plane is fixed as 30°. A total of 45 cases have covered a reasonable range of involved parameters and can present a full scope of the liquid bridge breakup process under various geometrical and wettability conditions. It is expected that upon reaching the hydrophilic conditions, the porous tips will behave as solid ones since the liquid penetration will be impeded.

RESULTS AND DISCUSSION

Simulation Results. By employing the proposed numerical model, the dynamics of a liquid bridge are simulated with different geometries and conditions. As shown in Figure 2, after touching the porous tip, the droplet infiltrates the porous zone driven by the capillary pressure and the apparent contact line outside the tip moves up along the oblique side, with the inside liquid front forming in a liquid bridge; when the solid plane is dragged far away from the porous tip, the contact line slips on the porous surface and tends to pinch while the liquid continues to imbibe. Once the liquid bridge breaks up, part of the outside liquid remains on the tip, while the other part is still attached to the plane. The ratio of the latter volume to the initial volume is defined as the liquid retention ratio L_r.

The simulation results, as shown in Figure 3, indicate that the liquid retention ratio L_r, covering a wide range from less than 0.4 to more than 0.9, is first controlled by the porous

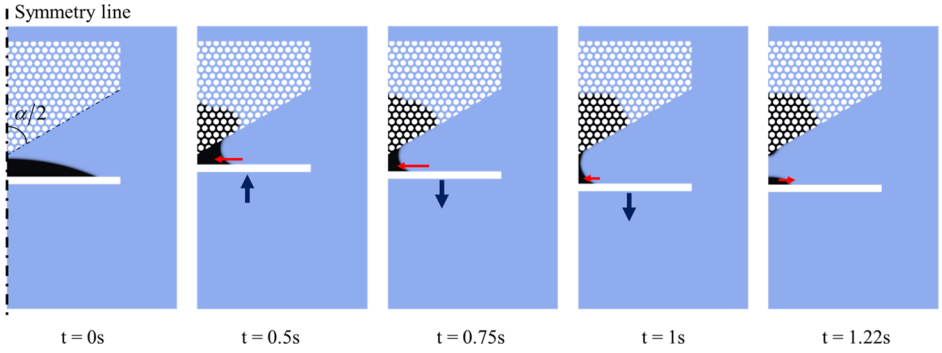

Figure 2. Schematic of the simulation model for porous tips and typical evolution of a liquid bridge with the loading time with α = 120° and u = 4 mm/s. The dark blue arrow indicates the moving direction of the bottom plate and the red arrow indicates the triple-phase line movement.

https://dx.doi.org/10.1021/acs.langmuir.0c02479
Langmuir 2020, 36, 13642−13648

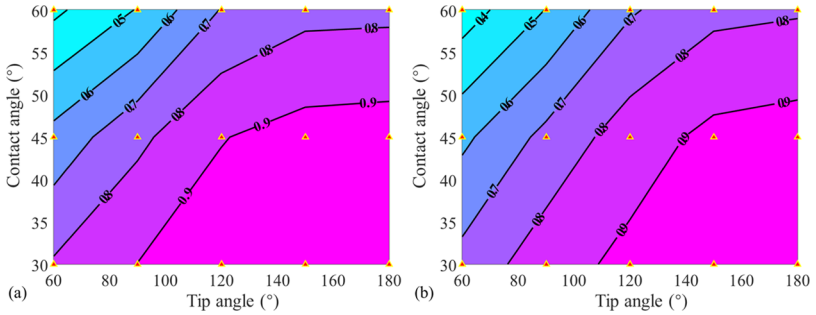

Figure 3. Smoothed contour plots of the liquid retention ratio with changing contact angle θ and tip angle α for different porosities ϕ: (a) 0.42 and (b) 0.49. The markers (▲) indicate the simulation cases.

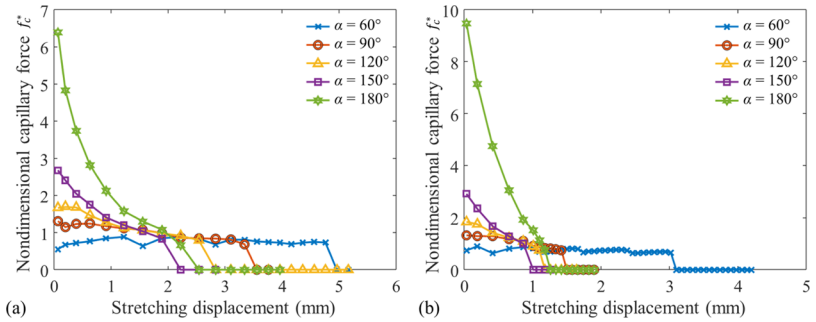

Figure 4. Nondimensional capillary force f_c^* vs stretching displacement with changing tip angle α for different stretching speeds u: (a) 4 mm/s and (b) 0.8 mm/s, with porosity ϕ = 0.42 and contact angle θ = 45°. Here, f_c^* is the ratio of per-unit-length capillary force of the moving plate and surface tension.

structure (porosity ϕ). Comparing Figure 3a,b, the contour lines shift to the top-left corner, i.e., L_r increases slightly when ϕ changes from 0.42 to 0.49 since the characteristic imbibition time determined by the combination of the permeability of porous zone k and capillary pressure P_c,[49] decreases correspondingly. Meanwhile, these two figures show similar trends of L_r for the combination of contact angle θ and tip angle α, i.e., the decrease of θ and increase of α result in more liquid retained on the tip. Specifically, for a given porosity, the smaller contact angle, i.e., the porous zone is more hydrophilic toward the liquid, leads to a higher capillary pressure or a lower characteristic imbibition time, which induces infiltration of the liquid into the porous tip. Together with porosity ϕ, contact angle θ determines the capillary effects on the dynamics of a liquid bridge. For the tip angle, macroscopically, it controls the slide of the contact line, as discussed in ref 8, i.e., the smaller the α, the easier it is for the contact line to move along the tip surface so that less volume of liquid would be retained on the tip at the moment of the rupture of a liquid bridge; microscopically, α also determines the diffusion area, which is specifically discussed in the following section. Figure 4 shows the variation of capillary forces applied on the solid object as a function of the stretching distance and speed until ruptures of the liquid bridge when the capillary force jumps to zero. Here, since the hydrostatic force is zero when ignoring the gravity effect, we calculate the capillary force by integrating the fluid pressure along the whole solid surface of the bottom plate. With increasing tip angle, the magnitude of capillary forces increases, while the rupture distance decreases. Also, the reduction range of capillary force from the initial state to rupture increases. Especially for α = 60°, the capillary force almost remains constant during the stretching since the contact lines adhered to the porous and solid surface slide at a similar pace so that the curvature of the gas−liquid interface does not change. Comparing Figure 4a,b, slowing the stretching speed results in the reduction of the rupture distance since imbibition as a competing factor of stretching dominates the liquid bridge rupture; specifically, more liquid infiltrates the porous zones during a relatively slower stretching process. This competition can be described by two characteristic time scales, as discussed in the following section.

Dimensionless Analysis. *Capillary-Driven Imbibition.* Assuming the contact area between the droplet and the porous tip as a point liquid source and the liquid front as a circular segmented centered on the point source, as shown in Figure 5, the infiltration area is

$$S_{imb} = \frac{1}{2}\phi H^2 \alpha \tag{9}$$

and according to the Lucas−Washburn equation,[49,50] within homogeneous porous media, the position evolution of liquid front H with time t can be estimated as

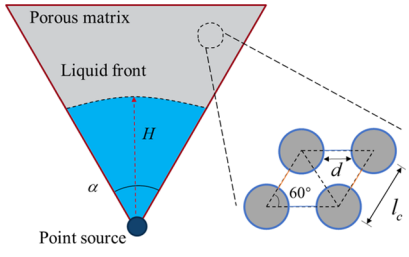

Figure 5. Schematic of a liquid-infiltrated porous tip with tip angle α.

https://dx.doi.org/10.1021/acs.langmuir.0c02479
Langmuir 2020, 36, 13642−13648

$$H^2 = \frac{2kP_c^*}{\phi\mu_l}t \tag{10}$$

where k and P_c^* are the permeability and characteristic capillary pressure of the porous tip, respectively. For the hexagonal arrangement of obstacles, as studied here, the permeability is a function of ϕ and d and can be estimated using the equation $k = d\cdot\frac{\phi^{0.76}}{1-\phi^{0.24}}$;[38] microscopically, the capillary pressure P_c is related to the contact line movement, i.e., filling angle φ, and the representative value of capillary pressure P_c^* can be estimated as a mean value of P_c, i.e.,

$$P_c^* = \frac{\int_{\alpha_0}^{\pi/2} P_c(\varphi)\mathrm{d}\varphi}{\pi} \tag{11}$$

More details about eq 11 can be found in ref 38.

Time Scales. The stretch velocity and capillary imbibition are two dominating factors in the liquid retention of a porous tip, and they can be related to respective characteristic time scales, i.e., macroscopic time length T_M and microscopic one T_m. A time ratio R_T as a dimensionless number is proposed here to link geometrical and flow conditions together. Specifically, T_M is the characteristic time during which the bottom solid substrate is dragged through a distance equaling the equivalent droplet size

$$T_M = \frac{r_d}{u} \tag{12}$$

where r_d is the initial size of a droplet; T_m is the time taken by the whole droplet to be imbibed by capillary suction of the porous tip, and thus setting the imbibition area S_{imb} equal to the droplet area, i.e., $1/2\pi r_d^2$. Combining with eq 10, T_m can be solved as

$$T_m = \frac{\pi r_d^2}{\alpha}\frac{\mu_l}{2kP_c^*} \tag{13}$$

Then, the original time scale ratio R_T^0 is expressed as

$$R_T^0 = \frac{T_M}{T_m} = \frac{2\alpha}{\pi r_d u}\frac{kP_c^*}{\mu_l} \tag{14}$$

Considering the deviation resulting from the assumption of the point source, a correction term related to the droplet size is proposed here

$$R_T = R_T^0\left(\frac{r_d}{d}\right)^n \tag{15}$$

where n is a fitting index. Based on eq 15, a larger R_T suggests that the external drag becomes slower or it takes less time for liquid to infiltrate into the porous tip, so the proposed R_T should be positively correlated with the liquid retention ratio, L_r.

Liquid Bridge Rupture. As suggested in ref 8, with the contact line movement on the solid surface, the liquid bridge finally breaks up and part of the liquid will be left on the tip, and the volume of the leftover is a function of tip geometry and surface property. However, for a porous tip, the imbibition inside the porous zone and outside stretching, as two competing factors, together impact the rupture of capillary bridges and liquid retention further, as shown in Figures 3 and 4. Similarly, the outside residual liquid induced by the capillary bridge breakup, contributing to the liquid retention ratio, is determined by tip angle α and contact angle θ and can be denoted R_S.

As analyzed above, the liquid retention ratio for a porous tip can be estimated as

$$L_r = R_S + (1 - R_S)f(R_T) \tag{16}$$

which includes two parts, i.e., the first term is the contribution of liquid bridge breakup and the second term is the additional retention induced by interior capillary effects. R_T, a time ratio defined above, is used to describe the capillary effect competing with the external stretching. It is observed from simulation results that more liquid is retained on the tip with the increment of R_T. Theoretically, when $R_T = 0$, suggesting that the capillary effect can be ignored and the liquid retention is identical to the one of a smooth solid tip, $f(0)$, therefore, should be zero; when $R_T \to +\infty$, i.e., the relative movement of the porous tip tends to stop ($u \to 0$) and the capillary-induced increment reaches the upper limit and $f(+\infty)$ should be 1. Thus, $f(R_T)$ can be formulated as

$$f(R_T) = \frac{e^{R_T/R_T^*} - 1}{e^{R_T/R_T^*} + 1} \tag{17}$$

where $R_T \in [0, +\infty)$, and correspondingly, $f(R_T) \in [0, 1)$. After the nonlinear regression analysis based on all of the obtained simulation data, containing 45 cases covering variations of tip geometry, wettability, and porous structures, the parameters R_T^* and n in the proposed correlation are fitted as 875.1 and 1.5, respectively, with $R^2 = 0.89$. The function of R_T as shown in eq 17 quantitatively characterizes the contribution of capillary effects to the liquid retention ratio and it is validated against our simulation results in Figure 6.

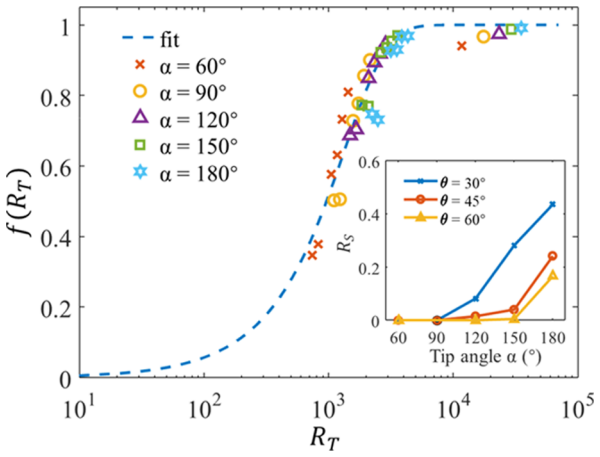

Figure 6. Simulation results and nonlinear regression curve of weight function $f(R_T)$. The inset presents the change of the contribution of liquid bridge breakup to the liquid retention ratio R_S with the tip angle α and contact angle θ.

In summary, the rupture of a liquid bridge is a complex dynamic process involving many parameters, including stretching speed, droplet size, wettability, tip shape, porosity, and pore size, that control such a process. However, these parameters related to the competition between capillary effects and external stretching can be combined as the proposed dimensionless number R_T. Regarding the involved physical lengths, i.e., size of the droplet and pore size, because the

https://dx.doi.org/10.1021/acs.langmuir.0c02479
Langmuir 2020, 36, 13642−13648

gravity effect is ignored in simulations, the droplet should be small enough to satisfy this assumption, whilst compared with the characteristic size of pore space, the droplet should be over 20 times larger than the throat size. The proposed expression regarding the liquid retention ratio in eq 16 combines two competing factors, i.e., imbibition inside the porous zone and contact line movement outside the porous zone. With the help of eq 16, we can predict the liquid retention ratio for the given geometry and flow conditions, and furthermore, for a given porous tip, we can also adjust the stretching speed to satisfy various liquid retention requirements. Conversely, the tip geometry, including tip angle and inner porous structure, can be designed based on the proposed relationship according to different application situations. A typical scenario can be implementation of multiple porous tips, with different design parameters (e.g., porosity and tip angle), in a system simultaneously to selectively manipulate droplets.

CONCLUSIONS

In this work, we studied the dynamics of a liquid bridge between a porous tip and a moving solid plane, and the impacts of capillary effects on the liquid transfer were investigated through a series of numerical simulations. Specifically, there are generally two volumes contributing to liquid retention during liquid bridge rupture. One is the imbibition into the porous tip, i.e., the initial droplet, as a liquid source, infiltrates the porous zone during stretching; the other is the contact line movement outside the porous tip, i.e., a part of the outside liquid is retained on the tip once the rupture occurs. We proposed a scaling parameter R_T, a time scale ratio, to quantify the relative contribution from capillary effects and then an estimation of liquid retention ratio L_r considering these two contributions is developed based on the simulation results. Notably, our estimation of L_r is consistent with the conclusion for solid tips (i.e., $R_T = 0$) reported in ref 8, whilst the proposed empirical equation can capture the additional contribution from the porous substrates. This study on rupture of liquid bridges suggests another potential way to accurately control liquid transfer and manipulate droplets required by microfluidics and microfabrication. Since the tip geometry has shown good potential in controlling the behavior of a liquid bridge, further investigation on the rupture mechanism of a liquid bridge adhered on a spherical porous domain, controlled by its local curvature, could be an extension of our current work.

AUTHOR INFORMATION

Corresponding Author

Yixiang Gan − *School of Civil Engineering, The University of Sydney, Sydney, NSW 2006, Australia;* orcid.org/0000-0002-9621-0277; Email: yixiang.gan@sydney.edu.au

Author

Si Suo − *School of Civil Engineering, The University of Sydney, Sydney, NSW 2006, Australia;* orcid.org/0000-0001-5704-5339

Complete contact information is available at: https://pubs.acs.org/10.1021/acs.langmuir.0c02479

Notes

The authors declare no competing financial interest.

REFERENCES

(1) Wu, Y.; Wang, F.; Selzer, M.; Nestler, B. Investigation of Equilibrium Droplet Shapes on Chemically Striped Patterned Surfaces Using Phase-Field Method. *Langmuir* **2019**, *35*, 8500−8516.

(2) Li, J.; Song, Y.; Zheng, H.; Feng, S.; Xu, W.; Wang, Z. Designing biomimetic liquid diodes. *Soft Matter* **2019**, *15*, 1902−1915.

(3) Wang, T.; Si, Y.; Dai, H.; Li, C.; Gao, C.; Dong, Z.; Jiang, L. Apex structures enhance water drainage on leaves. *Proc. Natl. Acad. Sci. U.S.A.* **2020**, *117*, 1890−1894.

(4) Sun, L.; Bian, F.; Wang, Y.; Wang, Y.; Zhang, X.; Zhao, Y. Bioinspired programmable wettability arrays for droplets manipulation. *Proc. Natl. Acad. Sci. U.S.A.* **2020**, *117*, 4527−4532.

(5) Matsui, H.; Noda, Y.; Hasegawa, T. Hybrid energy-minimization simulation of equilibrium droplet shapes on hydrophilic/hydrophobic patterned surfaces. *Langmuir* **2012**, *28*, 15450−15453.

(6) Liu, H.; Chu, F.; Zhang, J.; Wen, D. Nanodroplets impact on surfaces decorated with ridges. *Phys. Rev. Fluids* **2020**, *5*, No. 074201.

(7) Gurera, D.; Bhushan, B. Designing bioinspired conical surfaces for water collection from condensation. *J. Colloid Interface Sci.* **2020**, *560*, 138−148.

(8) Tourtit, Y.; Gilet, T.; Lambert, P. Rupture of a Liquid Bridge between a Cone and a Plane. *Langmuir* **2019**, *35*, 11979−11985.

(9) Wang, G.; Fei, L.; Luo, K. H. Lattice Boltzmann simulation of water droplet impacting a hydrophobic plate with a cylindrical pore. *Phys. Rev. Fluids* **2020**, *5*, No. 083602.

(10) Vourdas, N.; Pashos, G.; Kokkoris, G.; Boudouvis, A. G.; Stathopoulos, V. N. Droplet Mobility Manipulation on Porous Media Using Backpressure. *Langmuir* **2016**, *32*, 5250−5258.

(11) Pack, M.; Hu, H.; Kim, D.-O.; Yang, X.; Sun, Y. Colloidal Drop Deposition on Porous Substrates: Competition among Particle Motion, Evaporation, and Infiltration. *Langmuir* **2015**, *31*, 7953−7961.

(12) Hornbaker, D.; Albert, R.; Albert, I.; Barabási, A.-L.; Schiffer, P. What keeps sandcastles standing? *Nature* **1997**, *387*, No. 765.

(13) Vo, T.-T.; Mutabaruka, P.; Nezamabadi, S.; Delenne, J.-Y.; Radjai, F. Evolution of wet agglomerates inside inertial shear flow of dry granular materials. *Phys. Rev. E* **2020**, *101*, No. 032906.

(14) Masuda, Y.; Tomimoto, K.; Koumoto, K. Two-dimensional self-assembly of spherical particles using a liquid mold and its drying process. *Langmuir* **2003**, *19*, 5179−5183.

(15) Uran, S.; Šafarič, R.; Bratina, B. Reliable and accurate release of micro-sized objects with a gripper that uses the capillary-force method. *Micromachines* **2017**, *8*, No. 182.

(16) Lambert, P.; Seigneur, F.; Koelemeijer, S.; Jacot, J. A case study of surface tension gripping: the watch bearing. *J. Micromech. Microeng.* **2006**, *16*, 1267−1276.

(17) Hemeda, A. A.; Pal, S.; Mishra, A.; Torabi, M.; Ahmadlouydarab, M.; Li, Z.; Palko, J.; Ma, Y. Effect of Wetting and Dewetting Dynamics on Atomic Force Microscopy Measurements. *Langmuir* **2019**, *35*, 13301−13310.

(18) O'Connell, C. D.; Higgins, M. J.; Marusic, D.; Moulton, S. E.; Wallace, G. G. Liquid Ink Deposition from an Atomic Force Microscope Tip: Deposition Monitoring and Control of Feature Size. *Langmuir* **2014**, *30*, 2712−2721.

(19) Darhuber, A. A.; Troian, S. M.; Wagner, S. Physical mechanisms governing pattern fidelity in microscale offset printing. *J. Appl. Phys.* **2001**, *90*, 3602−3609.

(20) Kang, H. W.; Sung, H. J.; Lee, T.-M.; Kim, D.-S.; Kim, C.-J. Liquid transfer between two separating plates for micro-gravure-offset printing. *J. Micromech. Microeng.* **2008**, *19*, No. 015025.

(21) Wu, C. C.; Reinhoudt, D. N.; Otto, C.; Subramaniam, V.; Velders, A. H. Strategies for Patterning Biomolecules with Dip-Pen Nanolithography. *Small* **2011**, *7*, 989−1002.

(22) Curran, K.; Colin, S.; Baldas, L.; Davies, M. Liquid bridge instability applied to microfluidics. *Microfluid. Nanofluid.* **2005**, *1*, 336−345.

(23) Kok Keung Lye, J.; Wah, Ng. T.; Yeong Liang Ling, W. Discrete microfluidics transfer across capillaries using liquid bridge stability. *J. Appl. Phys.* **2011**, *110*, No. 104509.

(24) Wang, L.; Qiu, M.; Yang, Q.; Li, Y.; Huang, G.; Lin, M.; Lu, T. J.; Xu, F. Fabrication of microscale hydrogels with tailored microstructures based on liquid bridge phenomenon. *ACS Appl. Mater. Interfaces* **2015**, *7*, 11134−11140.
(25) Chen, H.; Tang, T.; Amirfazli, A. Fast Liquid Transfer between Surfaces: Breakup of Stretched Liquid Bridges. *Langmuir* **2015**, *31*, 11470−11476.
(26) Chen, H.; Tang, T.; Amirfazli, A. Effects of surface wettability on fast liquid transfer. *Phys. Fluids* **2015**, *27*, No. 112102.
(27) Kruyt, N. P.; Millet, O. An analytical theory for the capillary bridge force between spheres. *J. Fluid Mech.* **2017**, *812*, 129−151.
(28) Dai, Z.; Lu, S. Liquid bridge rupture distance criterion between spheres. *Int. J. Miner. Process.* **1998**, *53*, 171−181.
(29) Zhao, C.-F.; Kruyt, N. P.; Millet, O. Capillary bridges between unequal-sized spherical particles: Rupture distances and capillary forces. *Powder Technol.* **2019**, *346*, 462−476.
(30) Liang, Y.-E.; Weng, Y.-H.; Tsao, H.-K.; Sheng, Y.-J. Meniscus Shape and Wetting Competition of a Drop between a Cone and a Plane. *Langmuir* **2016**, *32*, 8543−8549.
(31) Darabi, P.; Li, T.; Pougatch, K.; Salcudean, M.; Grecov, D. Modeling the evolution and rupture of stretching pendular liquid bridges. *Chem. Eng. Sci.* **2010**, *65*, 4472−4483.
(32) Lian, G.; Thornton, C.; Adams, M. J. A theoretical study of the liquid bridge forces between two rigid spherical bodies. *J. Colloid Interface Sci.* **1993**, *161*, 138−147.
(33) Gupta, C.; Mensing, G. A.; Shannon, M. A.; Kenis, P. J. A. Double Transfer Printing of Small Volumes of Liquids. *Langmuir* **2007**, *23*, 2906−2914.
(34) Pitois, O.; Moucheront, P.; Chateau, X. Liquid bridge between two moving spheres: an experimental study of viscosity effects. *J. Colloid Interface Sci.* **2000**, *231*, 26−31.
(35) Lambert, P.; Delchambre, A. Parameters Ruling Capillary Forces at the Submillimetric Scale. *Langmuir* **2005**, *21*, 9537−9543.
(36) Rabinovich, Y. I.; Esayanur, M. S.; Moudgil, B. M. Capillary forces between two spheres with a fixed volume liquid bridge: theory and experiment. *Langmuir* **2005**, *21*, 10992−10997.
(37) Gambaryan-Roisman, T. Liquids on porous layers: wetting, imbibition and transport processes. *Curr. Opin. Colloid Interface Sci.* **2014**, *19*, 320−335.
(38) Suo, S.; Liu, M.; Gan, Y. Fingering patterns in hierarchical porous media. *Phys. Rev. Fluids* **2020**, *5*, No. 034301.
(39) Feng, S.; Shi, M.; Li, Y.; Lu, T. J. Pore-scale and volume-averaged numerical simulations of melting phase change heat transfer in finned metal foam. *Int. J. Heat Mass Transfer* **2015**, *90*, 838−847.
(40) Channon, R. B.; Nguyen, M. P.; Henry, C. S.; Dandy, D. S. Multilayered Microfluidic Paper-Based Devices: Characterization, Modeling, and Perspectives. *Anal. Chem.* **2019**, *91*, 8966−8972.
(41) Suo, S.; Liu, M.; Gan, Y. Modelling Imbibition Processes in Heterogeneous Porous Media. *Transp. Porous Media* **2019**, *126*, 615−631.
(42) Wang, Y.; Chen, K. S.; Mishler, J.; Cho, S. C.; Adroher, X. C. A review of polymer electrolyte membrane fuel cells: Technology, applications, and needs on fundamental research. *Appl. Energy* **2011**, *88*, 981−1007.
(43) Suo, S.; Liu, M.; Gan, Y. An LBM-PNM framework for immiscible flow: With applications to droplet spreading on porous surfaces. *Chem. Eng. Sci.* **2020**, *218*, No. 115577.
(44) Badalassi, V. E.; Ceniceros, H. D.; Banerjee, S. Computation of multiphase systems with phase field models. *J. Comput. Phys.* **2003**, *190*, 371−397.
(45) Yang, Q.; Li, B. Q.; Zhao, Z.; Shao, J.; Xu, F. Numerical analysis of the Rayleigh−Taylor instability in an electric field. *J. Fluid Mech.* **2016**, *792*, 397−434.
(46) Yang, Q.; Li, B. Q.; Ding, Y. 3D phase field modeling of electrohydrodynamic multiphase flows. *Int. J. Multiphase Flow* **2013**, *57*, 1−9.
(47) Yang, Q.; Li, B. Q.; Shao, J.; Ding, Y. A phase field numerical study of 3D bubble rising in viscous fluids under an electric field. *Int. J. Heat Mass Transfer* **2014**, *78*, 820−829.
(48) Shi, Z.; Zhang, Y.; Liu, M.; Hanaor, D. A.; Gan, Y. Dynamic contact angle hysteresis in liquid bridges. *Colloids Surf., A* **2018**, *555*, 365−371.
(49) Huinink, H. Two Phase Flow. In *Fluids in Porous Media: Transport and Phase Changes.*; Morgan & Claypool, 2016; pp 1−116.
(50) Washburn, E. W. The dynamics of capillary flow. *Phys. Rev.* **1921**, *17*, No. 273.

https://dx.doi.org/10.1021/acs.langmuir.0c02479
Langmuir 2020, 36, 13642−13648